

A stylized graphic consisting of a solid black shape on the left that tapers into a dashed line extending to the right. The text 'Research Report' is positioned to the left of this graphic.

Research
Report

Traction Drive System and its Characteristics as Power Transmission

Shuzou Sanda, Kisaburo Hayakawa

Abstract

Improvement in efficiency and durability is necessary for developing a traction drive continuously variable transmission (t-CVT). The traction coefficient at the power transmitting contacts of the t-CVT, which is the dominant factor in efficiency and durability, must be predicted with a high degree of accuracy and must be controlled in the design of a compact and efficient t-CVT. This report presents a new method of predicting the traction coefficient with sufficient accuracy.

In the prediction, a rheological model of the fluid film is simplified by separating a contact ellipse into three characteristic regimes in which

only one of the elastic, plastic, or viscous effect is dominant in each regime. This simplification makes it possible to obtain shear stress more easily than is possible with a direct numerical solution of a visco-elasto-plastic equation. A technique has also been developed to presume rheological properties from experimental traction curves with spin motion included, which is a condition corresponding to t-CVT contact.

With this method, the maximum traction coefficient can be predicted within 10% accuracy, which makes the optimum control of the normal force of the power transmitting contact of a t-CVT possible.

Keywords

Traction drive, Toroidal-CVT, Traction coefficient, Rheology, Spin loss, Control of clamping force

1. Introduction

Two types of continuously variable transmission (CVT), the push-belt type and the traction drive type, are currently being used. The traction drive CVT (t-CVT) is a power transmitting mechanism that uses the shear force between the rolling-sliding surfaces of rotating components.¹⁾ The advantages of the t-CVT when compared with the belt type CVT are less noise, greater response, and greater conformity with the front-engine rear-drive layout. Before traction drive can be developed as a leading type of CVT incorporating these advantages, efficiency and durability at the power transmitting contacts must be improved. Because the traction coefficient μ , which is the traction force divided by the normal force at the power transmitting contacts, is the dominant factor in efficiency and durability, the accurate prediction and control of μ is important for the design of compact and efficient t-CVTs.²⁾

Traction is the sum of shear stress in a lubricant film between two rolling elements resulting from the rheological behavior of a fluid under high pressure and high shear.³⁻⁸⁾ In actuality, the power transmitting contacts of a t-CVT inevitably include spin motion for realizing a continuous variation of speed. In this study, a new technique has been developed to determine the rheological properties of the fluid in which measured traction curves including spin motion are used in place of the traction curves of the 2- or 4-roller tester with no spin motion that was usually used in previous works.⁶⁻⁸⁾ A predictive model of μ with sufficient accuracy is constructed using the obtained rheological properties. The prediction makes possible the development of a controlling system of normal force at the power transmitting contacts.

2. Traction drive system

2.1 Principle of traction drive

Traction drive transmits power by the shear force of a lubricant film⁹⁾ with a traction fluid in an elasto-hydrodynamic state, at a few GPa of pressure and a thickness of several hundreds of nm, between two rotating components, as shown in Fig. 1. The viscosity of the traction fluid increases with increasing pressure. The pressure at which viscosity

begins to increase rapidly is called the glass transition pressure, the point at which the traction fluid changes into a hyaloid.¹⁰⁾ Generally, two rotating components are mutually and strongly pressed in order to exceed the glass transition pressure. The traction coefficient μ is then defined as the ratio of normal force F_c to traction force F_t , as shown in Eq. (1).

$$\mu = \frac{F_t}{F_c} \dots\dots\dots(1)$$

Compressive force (or clamping force) necessary at the power transmission contact, F_{cd} , is expressed as

$$F_{cd} = \frac{T}{\mu R_d} \dots\dots\dots(2)$$

where T is the transmission torque and R_d is the radius of rotation on the drive roller.

2.2 Power transmission systems using traction drive

Although a variety of traction drive mechanisms have been designed up to now, traction drive in this study is distinguished by the presence of spin in the power transmitting contacts which influences efficiency. Spin is a rotational slip element of the power transmitting contacts that is determined by a geometrical relation of the input and output rotating components. Spin becomes lost work if power is not transmitted and, as lost work, is converted to heat. Generally, it is difficult to avoid spin in the t-CVTs that can continuously change the speed ratio of the input and output rotating components. The relation between the shape of the rotating components and the presence of spin is shown in Table 1 for the contact of two rotating components. In the case where the rotational axes of two rotating components and the tangential line of the power transmitting contacts are parallel or intersect at one

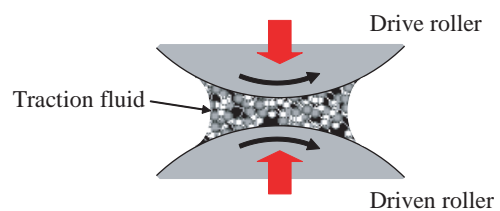


Fig. 1 Traction drive.

point, spin is not caused because the velocity distribution in the contact of two rotating components corresponds. In the case where this situation does not exist, spin is caused according to the difference of the velocity distribution.

As an example of a traction drive mechanism without spin, the planetary roller is well known as a Type I mechanism and is in commercial use for industrial, copy, and other types of machines.¹¹⁻¹³⁾ A Type II example is a taper roller applied to each of a sun roller, pinion roller, and ring. For example, if the ring is fixed, pushing the sun roller to the right causes the normal force for traction drive between two of the three rotating components due to the wedge effect.^{14, 15)} Moreover, a CVT in which a single disk is arranged transversely between two planetary rollers has been proposed.¹⁶⁾ An example of a traction drive mechanism with spin in current use is the Type III t-CVT.¹⁷⁾ This mechanism is explained in detail in Sect. 2. 3. The ring cone type

CVT¹⁸⁾ used in industrial machines is also a type III example. A double cone type CVT that clamps a ring between two cones and moves the ring in the direction of cone rotation axis has been proposed as a Type IV mechanism.¹⁹⁾

2. 3 Toroidal CVT (half/full) and its characteristics

The toroidal CVT available in cars today is one of the traction drive mechanisms described in Sect. 2. 2. The toroidal CVT was proposed by Charles W. Hunt in the 1870s. It had no practical applications because at that time it was a dry friction transmission, although attempts were made to use it as a vehicle transmission until about the 1920s. Thereafter, traction drive toroidal CVTs were developed and marketed for such uses as research in laboratories, bearings, oil, and cars. In 1999, Nissan and NSK were the first to mass-produce a toroidal CVT for automobiles.¹⁷⁾

The toroidal CVT has two forms, half toroidal and full toroidal,¹⁹⁾ determined by geometrical features. Figure 2 shows an example of each. In a full toroidal CVT, tilting axis of the roller between the input and output disks for changing transmission ratio is on the line on which the two contact points between the input and output disks and the roller are connected. Since the action force from the disk to the roller that is provided by the clamping force becomes the opposite direction and the same amount of force, the thrust force does not act on the bearing required to rotate the direction of power transmission in the roller. However, spin loss occurs at both the input and output contact because the tangent of the contact points might not intersect on the intersection of the rotating axes of the roller and the disk. Specifically, the velocity distribution in the contact ellipse on the disk is always different from that on the roller.

By contrast, the thrust force from clamping acts on the bearing required to rotate the direction of power transmission in the roller in a half toroidal CVT, because the tilting axis of the roller placed between the input and output disks for changing transmission ratio is not on the line on which the two contact points between the input and output disks and the roller are connected. The result is increased bearing loss. However, the spin loss at power transmission

Table 1 Category of traction drive.

Type	Spin loss			
	No		Yes	
	I	II	III	IV
Configuration of roller				
Velocity distribution on contact surface				

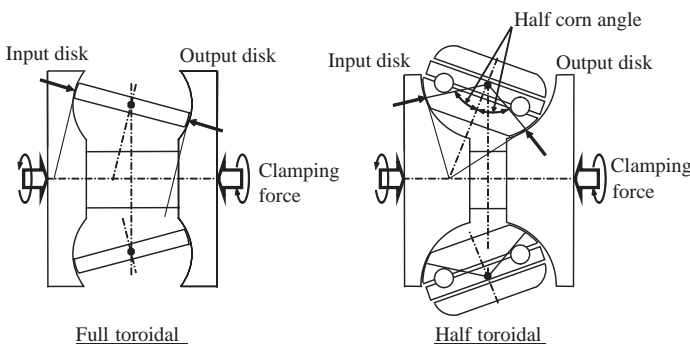


Fig. 2 Category of toroidal CVT.

contact is small because there is a state without spin in which tangents of the two contact points intersect on the axes of the input and output disks. Furthermore, the intersection is always in the vicinity of the axes of input and output disks even though the roller tilts in the direction that the transmission ratio changes. This spin loss increases and decreases according to the design values of the half cone angle and the cavity radius and other factors of the disk.

An example of the demand clamping force for traction drive is shown in **Fig. 3**. The clamping force of a full toroidal CVT is greater than that of a half toroidal CVT on the reduction side.

3. Analysis and prediction of traction characteristics

3.1 Overview of the rheology model and analysis

Traction force at a power transmitting contact is an integration of shear stress occurring due to resistance of the lubricant film at each point inside the contact ellipse. Evans et al.⁴⁾ proposed a generalized rheological map that shows a viscoelastic regime at lower pressures and an elasto-plastic regime at higher pressures. Ohno et al.⁵⁾ showed that the boundary of the viscoelastic and plastic regimes is determined by the product of the viscosity-pressure index α and pressure p .

Based on these results, the rheological model has been adopted as shown schematically in **Fig. 4**. At each point inside a contact ellipse, shear stress (τ_x, τ_y) appears due to the visco-elasto-plastic behavior of the fluid film, which has equivalent values of shear elasticity G , viscosity η , and limiting shear stress τ_L .

In previous studies,⁶⁻⁸⁾ measured traction curves by

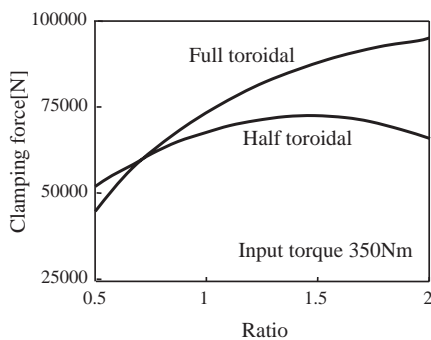


Fig. 3 Demand clamping force.

2- or 4-roller machines with no spin or skew motion were used to determine properties G , η and τ_L . However, power transmitting contacts in a t-CVT inevitably include spin motion. In this study, therefore, we present a new technique that presumes these properties from traction data that includes spin motion. We also propose a simplified rheological model that enables the calculation of shear stress without the difficulties involved in solving differential equations numerically. Precise methods for these are explained in the following sections.

3.2 Simplified rheological model and calculation of traction coefficient μ

To calculate shear stress (τ_x, τ_y) at each point in the contact ellipse, we propose the simplified model shown in **Fig. 5**. The contact ellipse is separated into three regimes in which only one of the properties, elasticity (G), plastic slip (τ_L), or viscous shear (η) is dominant. The dominant property is indicated by $\langle \rangle$.

- (I) No-slip regime with only elastic deformation $\langle G \rangle$
- (II) Plastic slip regime with limiting shear stress τ_L under high local pressure ($\alpha p \geq 25$) $\langle \tau_L \rangle$
- (III) Eyring viscosity regime under low local pressure ($\alpha p < 25$) $\langle \eta \rangle$

The boundary between regimes (II) and (III) is determined as $\alpha p = 25$ according to results by Ohno.⁵⁾ (τ_x, τ_y) satisfies the following basic equations,

$$\frac{U}{G} \frac{d\tau_x}{dx} + \frac{\tau_x}{\tau_e} F(\tau_e) = \frac{SU + \omega_s y}{h} \dots \dots \dots (3a)$$

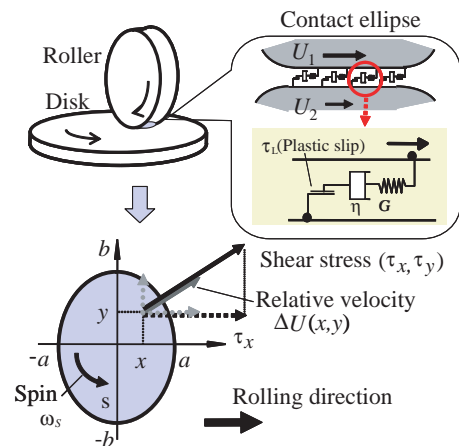


Fig. 4 Contact ellipse.

$$\frac{U}{G} \frac{d\tau_y}{dx} + \frac{\tau_y}{\tau_e} F(\tau_e) = -\frac{\omega_s x}{h} \dots\dots\dots(3b)$$

$$\tau_e = \sqrt{\tau_x^2 + \tau_y^2} \quad \sqrt{\tau_x^2 + \tau_y^2} \leq \tau_L \dots\dots\dots(4)$$

where

· Regime (II) Plastic: $F(\tau_e) = 0 \dots\dots\dots(5a)$

· Regime (III) Viscous:

$$F(\tau_e) = \frac{\tau_0}{\eta} \sinh\left(\frac{\tau_e}{\tau_0}\right) \dots\dots\dots(5b)$$

$$\tau_L = m p_{\max} \sqrt{1 - (x/a)^2 - (y/b)^2} \dots\dots\dots(6)$$

(τ_x, τ_y) : x and y component of shear stress

G : Equivalent shear elasticity

U : Mean rolling velocity = $1/2(U_1 + U_2)$

S : Slide roll ratio = $2(U_1 - U_2) / (U_1 + U_2)$

ω_s : Spin angular velocity

h : EHL film thickness²¹⁾

Boundary condition:

$$\tau_x = \tau_y = 0 \text{ at } (x/a) = -\sqrt{1 - (y/b)^2} \dots\dots\dots(7)$$

Solutions of (3a) to (7) with the above assumptions yield (τ_x, τ_y) in each regime in dimensionless forms as follows:

· Dimensionless parameters:

$$\frac{x}{a} = X, \frac{y}{b} = Y, \frac{a}{b} = \kappa, \frac{\tau_x}{m p_{\max}} = T_X, \frac{\tau_y}{m p_{\max}} = T_Y, \dots\dots\dots(8)$$

$$\frac{\tau_L}{m p_{\max}} = T_L, \frac{\tau_0}{m p_{\max}} = T_0, \frac{G a}{m p_{\max} h} = C^*, \frac{b \omega_s}{U} = \Omega_S$$

(I) No-Slip Regime:

$$T_X = C^* (S + \Omega_S Y) (X + \sqrt{1 - Y^2}) \dots\dots\dots(9a)$$

$$T_Y = \frac{1}{2} C^* \kappa \Omega_S (1 - X^2 - Y^2) \dots\dots\dots(9b)$$

where $\sqrt{T_X^2 + T_Y^2} \leq T_L \dots\dots\dots(9c)$

(II) Plastic slip regime ($\alpha p \geq 25$):

$$T_X = \frac{(S + \Omega_S Y)}{\sqrt{(\kappa \Omega_S X)^2 + (S + \Omega_S Y)^2}} \sqrt{1 - X^2 - Y^2} \dots\dots(10a)$$

$$T_Y = \frac{-(\kappa \Omega_S X)}{\sqrt{(\kappa \Omega_S X)^2 + (S + \Omega_S Y)^2}} \sqrt{1 - X^2 - Y^2} \dots\dots(10b)$$

where $\sqrt{T_X^2 + T_Y^2} \geq T_L \dots\dots\dots(10c)$

(III) Viscous slip regime ($\alpha p < 25$)

Only a numerical solution is available.

The traction coefficient is obtained from T_X as follows:

$$\mu = \frac{\iint_{\text{Contact ellipse}} \tau_x dA}{W} = \frac{3m}{2} \iint_{\text{Contact ellipse}} T_X dXdY \dots\dots(11)$$

where W : Normal force = $(3/2)\pi ab P_{\max}$.

Next, the actual values of the equivalent rheological properties G , η , and τ_L are determined. G and η are assumed as follows:

(1) Elasticity G

$$G = (Gf^{-1} + G_S^{-1})^{-1} \dots\dots\dots(12)$$

where

$Gf = (2\pi \sim 30)\tau_L$: fluid film component of G

$G_S = 0.56Eh/\sqrt{ab}$: rolling element component of G

Estimation of each value leads to

$$G \approx G_S = 0.56Eh/\sqrt{ab} \dots\dots\dots(13)$$

(2) Viscosity η : Eyring's model with Barus'

pressure viscosity relation is used.⁵⁾

$$\dot{\gamma} = \frac{\tau_0}{\eta} \sinh\left(\frac{\tau}{\tau_0}\right) \dots\dots\dots(14)$$

$$\eta = \eta_0 \exp(\alpha p) \dots\dots\dots(15)$$

where τ_0 : Eyring stress $\dot{\gamma}$: Shear rate

η_0 : Viscosity at standard pressure

α : Viscosity-pressure index by Barus

η_0 and α are ordinarily given as empirical equations. τ_0 is presumed from experimental data, as mentioned later.

3.2 Estimation of rheological properties

In contrast with previous studies⁶⁻⁸⁾ that use traction data by 2- or 4-roller testers with no spin or

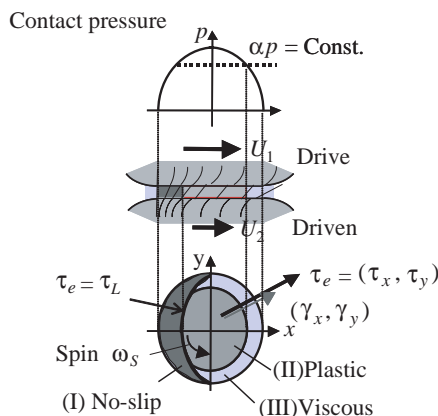


Fig. 5 Simplified rheology model.

skew motion, τ_0 and τ_L are successfully presumed in this study from traction data that includes spin motion.

The test apparatus and conditions are shown in **Fig. 6** and **Table 2**. A test contact point is formed between a disk and a roller with axes perpendicular from each other and connected in a power circulation loop. The slide-roll ratio at the test contact is set by a CVT in the power circulation loop. Torque on the roller axis is measured to obtain the traction force. Spin rate is varied under the same mean rolling speed by changing the radial position of the test contact on the disk.

Figure 7 shows an example of measured traction curves. The gradient of the traction curves of the same mean rolling velocities varies with the spin rate at a lower slide-roll ratio.

Limiting shear stress τ_L is presumed from these data as follows. Assuming that the whole contact ellipse reaches plastic flow regime (II), Eqs. (10) and (11) yield

$$\mu = \frac{F}{W} = \frac{\text{contact area}}{\frac{2}{3} \pi ab p_{\max}} = \frac{3m}{\pi} A(\beta, \kappa) \quad \dots\dots\dots(16a)$$

$$A(\beta, \kappa) = \iint_{\text{contact area}} \frac{\sqrt{1-X^2-Y^2} \tau_x}{\sqrt{(\beta+Y)^2 + (-\kappa X)^2}} dA \quad \dots\dots\dots(16b)$$

where β is defined as the "generalized slide-roll ratio"

$$\beta = \frac{SU}{b\omega_s} = \frac{S}{\Omega_s} \quad \dots\dots\dots(17)$$

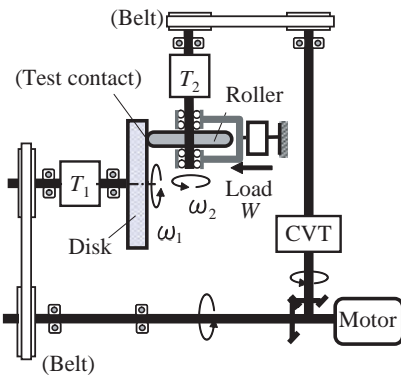


Fig. 6 Traction test apparatus.

Equations (16a) and (16b) show that the "generalized" traction curves depend merely on β and the aspect ratio of the contact ellipse $\kappa = a/b$. The distribution of the relative velocity, $\Delta U(x, y)$, is similar at the same value of β . For example, $\Delta U(x, y)$ distributes as triangular on the transverse axis $x=0$ at $\beta = 1$ (shown in **Fig. 8**). Accordingly, the "generalized" traction curves of different spin rates are necessarily the same as those shown in Fig. 8 except at a higher slide-roll ratio, where the effect of temperature rise by frictional heating is dominant.

From Eq. (16), $m (= \tau_L / p)$ is expressed using the representative traction coefficient μ^* at $\beta=1$.

$$m = \frac{\tau_L}{p} = \frac{\pi \mu^*}{3C} \quad \dots\dots\dots(18a)$$

Table 2 Test conditions.

Contact radius on disk	R_1	30 ~ 80 mm
Roller radius	R_2	50 mm
Mean rolling velocity	U	5 ~ 20 m/s
Spin angular velocity	ω_s	66 ~ 335 rad/s
Normal load	W	1 ~ 10 kN
Max. hertzian pressure	P_{\max}	0.9 ~ 3.0 GPa
Roller crowning radius	R_C	5, 20, 75 mm
Supply fluid temperature		60, 80, 100 °C

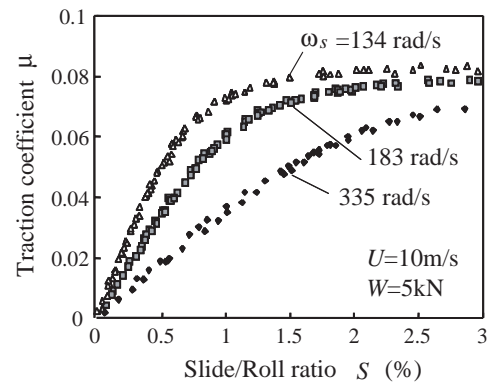


Fig. 7 Measured traction curves.

$$C = \iint_{\text{contact area}} \sqrt{1-X^2-Y^2} \tau_x \frac{1+Y}{\sqrt{(1+Y)^2 + (-\kappa X)^2}} dA \quad \dots (18b)$$

C is only a function of $\kappa=b/a$.

The obtained m by (18a) is plotted versus $\alpha\bar{p}$ as shown in **Fig. 9** (\bar{p} : mean Hertzian pressure). m tends to increase with an increase of $\alpha\bar{p}$ at $\alpha\bar{p} < 25$, while it is almost constant at $\alpha\bar{p} > 25$, which agrees well with the results by Ohno⁵⁾. Hence, only data in $\alpha\bar{p} > 25$, presumed to be in the elasto-plastic zone, are valid in obtaining m from Eq. (16a). **Figure 10** shows these data plotted versus oil film temperature T_f , which is presumed from the measured roller surface temperature just after the test contact, and temperature rise due to frictional heating estimated as follows:

$$\Delta T = \frac{\sum(\text{Power loss})}{\pi ab} \left(\frac{0.48a}{\sqrt{\pi} \lambda \rho c a U_m} + \frac{hc}{16\lambda_L} \right) \quad \dots (19)$$

where

λ, λ_L : Heat conductivity of surface material and fluid

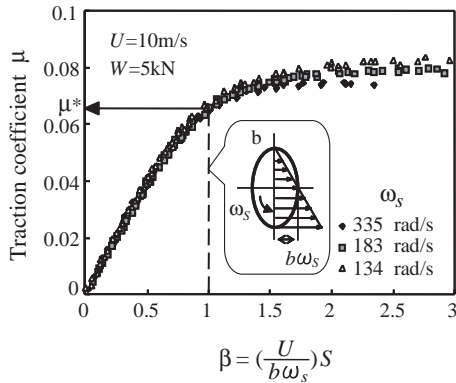


Fig. 8 Generalized traction curves.

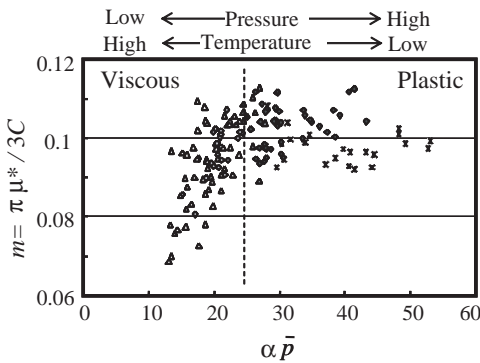


Fig. 9 Rheological regimes.

ρ, c : Density and specific heat of surface material
 hc : EHL central oil film thickness²¹⁾

Σ (Power loss): Total power loss in a contact ellipse

Estimated m tends to decrease slightly with the rise of T_f , which almost agrees with the results by Evans et al.⁴⁾ The empirical equation of m is also shown in Fig. 10.

Eyring stress τ_0 can also be presumed empirically from the data at $\alpha\bar{p} < 25$ in Fig. 9. Equation (14) derives

$$\frac{\tau}{\tau_0} = \sinh^{-1} \left(\frac{\eta \dot{\gamma}}{\tau_0} \right) \cong \ln \left(\frac{2\eta \Delta U}{\tau_0 hc} \right) \quad \dots (20)$$

$$\tau_x = \frac{(c+y)}{\sqrt{(c+y)^2 + (-x)^2}} \ln \left(\frac{2\eta \Delta U}{\tau_0 hc} \right) \quad \dots (21)$$

The traction coefficient is expressed as

$$\mu = \frac{2\tau_0}{\pi \bar{p}} \left[B_1(\beta, \kappa) \cdot \ln \left(\frac{2\eta \Delta U}{\tau_0 hc} \right) + B_2(\beta, \kappa) \right] \quad \dots (22a)$$

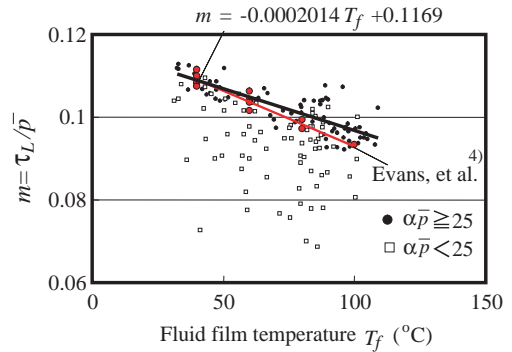


Fig. 10 Presumption of limiting shear stress.

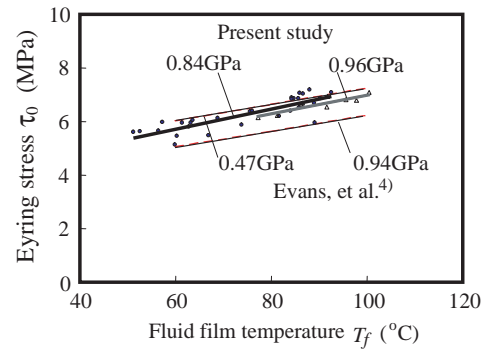


Fig. 11 Presumption of Eyring stress.

where

$$B_1(\beta, \kappa) = \iint_{(\text{contact area})} \frac{\beta + Y}{\sqrt{(\beta + Y)^2 + (-\kappa X)^2}} dA$$

$$B_2(\beta, \kappa) = \iint_{(\text{contact area})} \frac{(\beta + Y) \ln \left(\sqrt{(\beta + Y)^2 + (-\kappa X)^2} \right)}{\sqrt{(\beta + Y)^2 + (-\kappa X)^2}} dA \quad \dots \dots (22b)$$

τ_0 and μ^* satisfy the following relation:

$$\frac{\mu^* \bar{p}}{\tau_0} = \frac{2}{\pi} \left[B_1(1, \kappa) \cdot \ln \left(\frac{2\eta \Delta U}{\tau_0 hc} \right) + B_2(1, \kappa) \right] \quad \dots \dots (23)$$

The numerical solution of Eq. (23) yields τ_0 . The empirical relation between τ_0 and T_f is shown in Fig. 11. Estimated τ_0 tends to increase slightly with the rise of temperature T_f , which also agrees with Evans et al.⁴⁾ This agreement of the results suggests the reliability of the present methodology.

3.4 Calculation of traction and its verification

Traction coefficient μ is predicted using the present methodology at each operating condition of t-CVT. The contact ellipse radii and pressure distribution are calculated by Hertzian theory from the variator specification, transmission ratio, input torque, and revolution.²⁾ Since rheological properties change with the fluid film temperature T_f , determined by frictional heating by power loss, iteration is necessary for calculating μ and T_f simultaneously. The algorithm is shown schematically in Fig. 12.

Figure 13 shows a representative prediction of traction curves. Figure 14 compares the predicted maximum traction coefficient μ_{\max} with the

measured values. The accuracy is within 10% in most operating conditions of a t-CVT. This study is the first to achieve this level of accuracy for such broad conditions as pressure up to 3 GPa and velocity up to 20m/s.

3.5 Application of μ_{\max} prediction to normal force control

The demand clamping force for traction drive (state of μ_{\max}) changes according to structure, rotating speed, temperature of the oil film, input torque, and other factors as described in Sect. 3. 4. For example, the demand clamping force of the toroidal CVT shown in Fig. 3 changes according to the speed ratio. Consequently, control of the clamping force depending on speed ratio prevents excessive clamping force and gross slipping due to insufficient clamping force. It is also possible that controlling the clamping force raises the transmission efficiency and extends the life of the disk and roller.

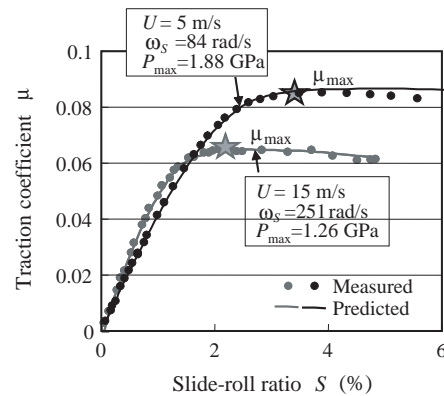


Fig. 13 Predicted traction curves.

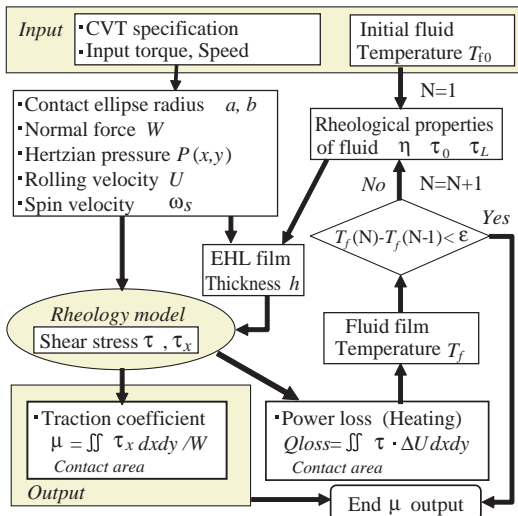


Fig. 12 Algorithm of traction calculation.

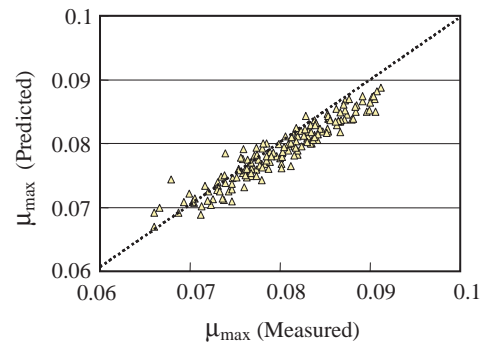


Fig. 14 Verification of prediction μ_{\max} .

Figure 15 shows an example of an oil pressure control system for clamping. The safety factor SF is set based on μ_{\max} calculated with the algorithm in **Chapt. 3** with respect to a rapid torque change, and parameter changes of the hydraulic apparatus and target traction coefficient $\mu_r = \mu_{\max}/SF$ are calculated. In addition, the demand clamping force is calculated based on μ_r and the estimated input torque. The oil pressure required to generate the demand clamping force is calculated, and the control signal is input to the oil pressure control valve.

4. Summary

A predictive method for traction coefficient μ at the power transmitting contacts of a toroidal CVT has been developed. The method has the following advantages:

- (1) Simplified rheological model that separates a contact ellipse into three regimes, elastic, plastic and viscous, to make calculation of shear stress easier.
- (2) A technique for presuming rheological properties from traction curves that include spin motion.

With this method, the maximum traction coefficient can be predicted within 10% accuracy, making optimum control of the normal force of the power transmitting contact of a t-CVT possible.

Recently, there has been work on developing a molecular simulation of the traction fluid.²³⁾ The simulation is expected to clarify rheological behavior of the fluid at the nanoscale level and to

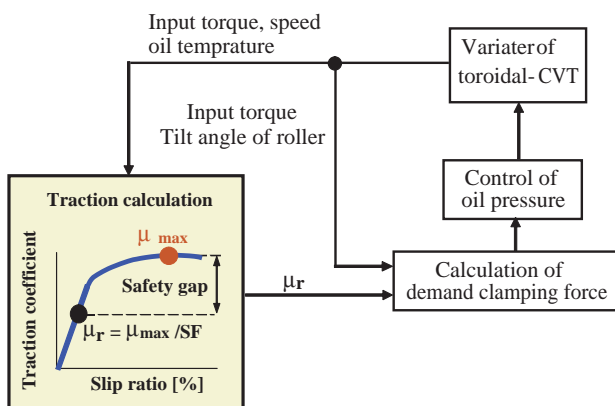


Fig. 15 Control system of clamping force.

result in the near future in a new predictive method of macroscopic rheological behavior.

Acknowledgments

The authors wish to acknowledge the support of Mr. T. Sano and other members of Toyota Motor Corporation. The authors also acknowledge contributions from T. Suzuki, T. Abekura, M. Kuroishi, and other members of the TCRD.

References

- 1) Machida, H., et al. : NSK Tech. J., No. 669 (in Japanese), (2000), 9-20
- 2) Tanaka, H. : Toroidal CVT (in Japanese), (2000), *Korona Sha*
- 3) Johnson, K. L., et al. : Proc. Roy. Soc. London A, **356**(1977), 215
- 4) Evans, C. R. and Johnson, K. L. : Proc. Inst. Mech. Eng., **200-C5**(1986), 313
- 5) Ohno, N., et al. : J. Jpn. Soc. Tribologists, **33-12** (1988), 922 (In Japanese)
- 6) Muraki, M. : J. Jpn. Soc. Tribologists, **46-5**(2001), 355 (In Japanese)
- 7) Makino, T., et al. : Trans. ASME J. Tribology, **121-2** (1999), 286
- 8) Ushijima, K., et al. : 2000 JSME Ann. Meet. in Nagoya, (In Japanese), (2000), 365
- 9) Heilich, F. W. III and Shube, E. : Traction Drives, (1983), 5, Marcel Dekker, Inc.
- 10) Jacobson, B. O. : Rheology and Elastohydrodynamic Lubrication, (1991), 92, Elsevier, Tribology series
- 11) Takahashi, H., et al. : United States Patent, 4483216
- 12) Showa Tool Co., TLD., "Traction Drive Speed Accelerator", SHOWATOOLNET, (online), available from <<http://www.showatool.com/en/traction/index.html>>, (accessed 2005-6-17)
- 13) NSK Corp., "Wedge Roller Traction Drive Unit", NSKNET, (online), available from <<http://www.us.nsk.com/images/e4202catalog.pdf>>, (accessed 2005-6-17)
- 14) Dell, C. and Red, H. L. : United States Patent, 1993051
- 15) Nakamura, Y., et al. : "Evaluation of High Efficiency Tapered Planetary Roller Traction Drive", *Nihon Kikai Gakkai 1999 Nen Nenji Taikai Kouen Ronbunshu*, (1999), 291, JSME
- 16) Young, J. R. & Young, J. D. : SAE Tech. Pap. Ser., No.2001-0356(2001), 49
- 17) Kumura, H., et al. : "Development of a Dual-Cavity Half-Toroidal CVT", Proc. of CVT99, Eindhoven, (1999), 65
- 18) *Nippon Densan Simpo*, "Ring Cone CVT", SHIMPONET, (online), available from <<http://www.shimpo.com>>, (accessed 2005-6-17)
- 19) GIF, "Transmission Development", GIF-ACNET, (online), available from

<http://www.gif-ac.com/html/transmission_productdetails1_e.php3>,
(accessed 2004-6-3)

- 20) Fellows, G. T. and Young, D. C. : SAE Tech. Pap. Ser., No.910408(1991), 9
- 21) Chittenden, R. J., et al. : Proc. Inst. Mech. Eng. Part C, **200**-3(1986), 219
- 22) Kakuta, K. : J. Jpn. Soc. Tribologists, **42**-7(1997), 590 (In Japanese)
- 23) Washizu, H., et al. : Synopses of Int. Tribology Conf., Kobe, (2005), 350

(Report received on July 12, 2005)



Shuzou Sanda

Research fields : Tribology in automotive power train components
Academic degree : Dr. Eng.
Academic society : Jpn. Soc. Tribol., Jpn. Soc. Mech. Eng., Soc. Autom. Eng. Jpn.



Kisaburo Hayakawa

Research fields : Estimation, control, modeling and analysis of power transmission system
Academic degree : Dr. Eng.
Academic society : Soc. Instrum. Control Eng., Jpn. Soc. Mech. Eng., Soc. Autom. Eng. Jpn.